H.P. Summers, M. von Hellermann, F. de Heer, R. Hoekstra
and JET Team

The Requirements for Collision Data on the Species Helium, Beryllium and Boron in Magnetic Confinement Fusion

The Requirements for Collision Data on the Species Helium, Beryllium and Boron in Magnetic Confinement Fusion

H.P. Summers, M. von Hellermann, F. de Heer[1], R. Hoekstra[2]
and JET Team*

JET-Joint Undertaking, Culham Science Centre, OX14 3DB, Abingdon, UK

[1]*AMOLF, Kruislann, Amsterdam*
[2]*KVI, Zemikelaan, Groningen*
* See Annex

ABSTRACT.

Requirements for collision data on helium, beryllium and boron are reviewed in the light of the directions of present and planned tokamak fusion experiments. The occurrence of the atoms and ions of these species and their roles in plasma behaviour and diagnostic measurements are described. Special emphasis is placed on alpha particle detection in reacting plasmas and beryllium and boron in divertor configuration machines. The atomic reactions required to exploit the species in models and diagnostic analysis are gathered together and their relative importances indicated. The article is intended as an introduction to the detailed studies of collision cross-sections presented in the other works in this volume.

1. INTRODUCTION.

Although the usual primary species in present tokamak fusion experiments is deuterium and in future ignited plasma experiments such as ITER will be a 50% mixture of deuterium and tritium isotopes, it is well known that other elemental species play a crucial and sometimes decisive role in plasma behaviour. Helium, beryllium and boron are of particular importance. Beryllium is the element of lowest Z with conductive and thermal properties which make it a possible plasma facing surface material for fusion reactors. As such, it has been under test at JET as a ~ few hundred monolayer coating from evaporators, as a solid limiter and as strike zone plates in X-point operation [1]. It will be used initially as the dump plates in the pumped divertor structure under assembly at JET. Boron on the other hand, deposited on carbon facing surfaces by, for example, glow discharges in B_2H_6 mixtures [2], appears to confer benefits similar to solid beryllium. That is in gettering oxygen and achieving low Z_{eff} and radiant losses in the plasma. 'Boronisation' is a widely used strategm at this time in most carbon first wall based fusion experiments such as TEXTOR and JT60. Helium is different. It is the product of the tritium/deuterium fusion reaction, that is, the internal kinetic energy source and the spent fuel of the self-sustaining reacting plasma. Retention and redistribution of the alpha particle birth energy amongst the plasma ions and then the transport, recycling and exhaust of the thermal alpha particles are evidently key issues for a reactor [3] [4]. Previous collections of atomic data for helium include Janev et al. [5], while atomic data for edge studies have been reviewed by Janev et al. [6].

An objective of this volume is to assemble and improve the atomic collision data required for modelling helium, beryllium and boron in the reactor regime. It is essential however that such data are extended to and are consistent with those used in studies of the present generation of sub-critical fusion devices. It is in these devices that models and behaviours of the species are under experimental test. It must also be recognised the species play a dual role in a plasma, namely, as components in the overall plasma models on the one hand, and as diagnostic probes of plasma parameters in their own right on the other. In seeking to provide a commonality of sound atomic collision data for helium, beryllium and boron, a working principle is that data for modelling should be dressed with a consistent set of data which supports associated experimental diagnosis.

The following two sections describe the occurrence and behaviour of helium and then beryllium and boron respectively in fusion plasmas. Methods for their measurement and their exploitation in a diagnostic sense, which use atomic collisions, are also examined. Then in the fourth and fifth sections, detailed ranked lists of atomic reactions are assembled to support these aspects. Also an indication of the accuracy with which the associated cross-sections need to be known is given. The study is heavily weighted towards helium and alpha particle detection using helium beams. Deuterium beams, associated beam stopping and D/He^{+2} charge exchange have been described in detail before and are excluded. Likewise, broad ionisation, recombination and radiated power under electron collisions of light species are already familiar and so detail in this area is reduced and mostly new aspects only are emphasised.

2. ASPECTS OF HELIUM AND ITS MEASUREMENT.

The presence of helium in the plasma arises four ways. Firstly, it can be introduced in the intial gas fill for the discharge. Usually this is as a minor constituent (~ 5% of either ^3He or ^4He) for coupling

ion cyclotron radio frequency power to the plasma. It can be introduced by gas puffing at the periphery of the plasma during a discharge, principally as an edge probe (see for example results on TEXTOR [7]). Fast $(E \gtrsim 30 keV/amu)$ neutral beams of ^3He and ^4He are used at JET for heating and deep helium deposition [8] and similar but less powerful beams are also used as diagnostic beams (for example $E \sim 15 keV/amu$ at TFTR and $E \lesssim 50 keV/amu$ at JT60 [9]). A diagnostic beam at $E \gtrsim 50 keV/amu$ has been suggested for ITER. Finally, deuterium/tritium fusion will provide a fast alpha particle source $(E \sim 880 keV/amu)$ in the core of a reacting plasma. These various sources result in a range of different distributions in space and velocity space.

The stationary radial thermal alpha particle distribution reflects the balance of ionisation, recombination, transport and then the sources and recycling parameters of helium in a plasma. The ionisation state of thermal helium is maintained primarily by electron collisions although at the highest ion temperatures achieved $(T_i \gtrsim 30 keV)$ ionisation by ion impact becomes important. The first two ionisation stages, He^0 and He^{+1}, are strongly edge localised while He^{+2} extends over the whole plasma volume.

The fusion alpha particles by contrast are expected to display a 'slowing down' distribution function confined primarily to the hot central part of the plasma (see however [10]. for more detail). It is parametrised essentially by the source rate and the critical speed at which slowing by collisions with electrons gives way to ion scattering and the slowing distribution merges with the thermal alpha particle distribution.

In ion cyclotron resonance heating of the plasma, the minority alpha particles are accelerated to high energies $\lesssim$ few MeV and diffuse and slow down away from the absorbing layer. Thus they are expected to have a slowing distribution function somewhat similar to the fusion alpha particles, but with different spatial aspects depending on the location of the layer. The details of the ICRF driven alpha particle distributions have been described in [11]. To a degree therefore, ICRH accelerated alpha particle distributions provide a test area for fusion alpha particle detection methods.

The He^0 atoms in a neutral beam show an exponential attenuation into the plasma due to ionising and charge exchanging collisions with plasma ions. (The beam has in general significantly populated $2\,^1S$ and $2\,^3S$ metastable state populations as well as the ground state $1\,^1S$. Attenuation of the metastable populations is quite different from that of the ground population.) For fast penetrating beams with energies $\gtrsim$ 20keV/u, electron collisions are less effective than ion collisions in this. Also the beams atoms are themselves excited in such collisions and radiate. This gives the 'beam emission spectrum' [12]. The beam/plasma interaction creates a number of secondary populations, namely:-

(a) Halo atoms - these are D^0_{plasma} atoms formed by the charge exchange reaction between D^+ and He^0 in the beam. They migrate in a random walk by further CX reactions until ionised. Typically they are localised within $\sim$ 30cm of the beam itself for plasma temperatures $\sim$ 15keV.

(b) Prompt and plume ions - these are $X^{+z_0 - 1}$ ions such as He^{+1} formed by charge exchange reactions between X^{+z_0} and He^0 in the beam. It is helpful to distinguish the initially formed ions in excited states (prompt) which radiate rapidly and the ground state ions which travel significant distances along field lines (plume). The former give the 'charge exchange spectrum'. The latter, re-excited by electron collisions, can again radiate before finally ionising in positions away from their point of formation (in JET, $\sim$ 40m for C^{+5} and $\sim$ 6m for He^{+1} at 5keV & 5.0^{13} cm^{-3}) [13].

(c) The slowing down ionised beam population. For example, for $^3He^0$ beams at 50 keV/amu in JET, the slowing down time of the fast $^3He^{+2}$ after double ionisation is $\sim$ .3 - .6 sec. This population behaves in a similar manner to the fusion alpha particles in the late phase of their slow down. There is also the singly ionised He^{+1} population in this group which is essentially a plume and distinguished from (b) only by its fast speed distribution [14]. Plasma ion and electron collisions are effective in destroying this population by reionisation and charge exchange.

(d) Neutralised fast alpha particles created by the double charge transfer reaction between He^{+2} and He^0. These particles can in principle escape from the plasma, but are attenuated by reionising and charge exchanging collisions with plasma ions in a manner similar to the neutral helium beams themselves. Neutralised thermal alpha particles will also be formed but are of less interest.
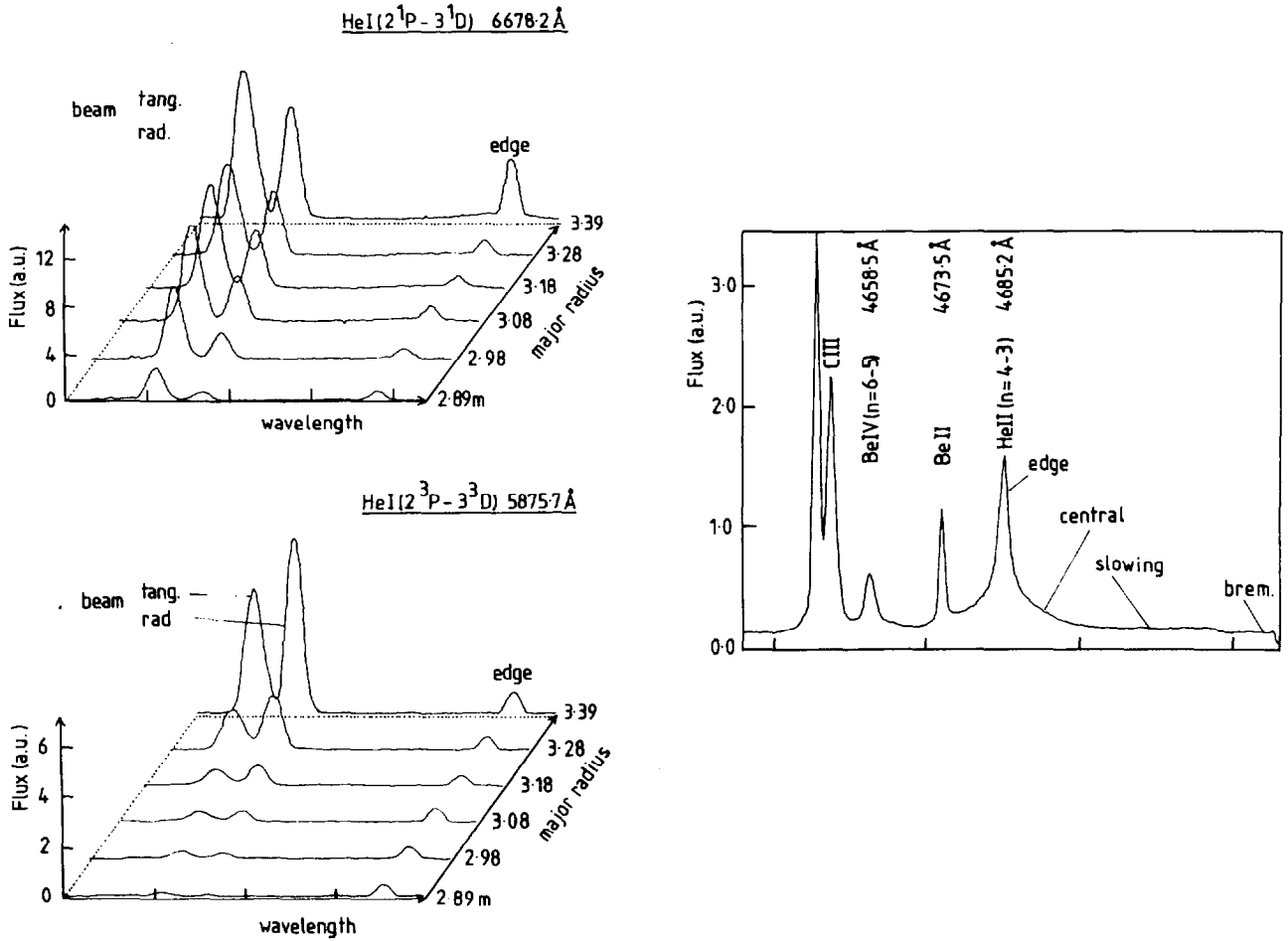

Fig. 1. (a) Spectral observation through the JET He^3 beams in the vicinity of $HeI(2\ ^1P - 3\ ^1D)$ $\lambda6678$Å. Note the emission from the edge at the nominal wavelength and the Doppler shifted beam emission. The Doppler shift varies with viewing angle into the plasma. 3.39m is near the outer edge of the plasma and 2.89m halfway to the centre. Note a JET injector has two beamline stacks at different inclinations to the viewing direction. The attenuation into the plasma is evident. (b) Similar observation of the vicinity of $HeI(2\ ^3P - 3\ ^3D)$ $\lambda5876$Å. Note the more rapid attenuation due to the ease of ionising the 2^3S metastable. (c) Spectral observation through the He^3 beams showing edge plasma emission $(CIII, HeII, BeII, BeIV)$. Note the broader $HeII(n = 4 - 3)$ $\lambda4685$Å charge exchange spectroscopy component from the plasma centre and the very broad pedestal. The latter is a slowing down feature associated with the helium beams. It is probably partly ionising He^+ beam plume ions and partly the subsequent circulating fast He^{+2} ions recombining through charge exchange. $BeIV(n = 6 - 5)$ has also a broadened CX component.

4

Turning to measurement of these populations, since the alpha particles are non-radiating and confined in the plasma, this must be enabled by an electron capture. Two routes for such measurement are double charge transfer (neutralisation) followed by external neutral particle detection and energy analysis, and single charge transfer followed by analysis of the cascade radiation of the He^{+1} particle. Projection of solid pellets of lithium into a plasma has been suggested as a means of providing a high concentration of suitable donors [15]. Penetrating neutral helium beams also provide suitable donors in the core of the plasma because of the efficiency of the resonant double charge transfer reaction. Neutral beam driven detection only is addressed here. It is noted that a 50keV/u diagnostic neutral helium beam has been proposed to enable neutral particle detection on ITER and a 100keV/u deuterium beam as a charge exchange diagnostic, although modification of ITER plans continue. Because of the size and densities of the expected ITER plasma, a 50 keV/u He^0 beam would only penetrate one quarter of the way to the centre of the ITER plasma. Helium beams, of course, also allow the spectroscopic approach (see [12]). Detection of neutralised alpha particles using neutral helium beams depends on (i) penetration of the neutral helium beam to the point of collision with an alpha particle, (ii) neutralising of the alpha particle by double charge transfer, (iii) escape of the He^0 from the plasma for measurement. Recent results at JT60 and JET are given in [9] and [16]. The charge exchange spectroscopy measurement also depends on (i), but (ii) is replaced by single charge transfer and the emitted photons escape without loss. Neutral particle detection and charge exchange spectroscopy are complementary. Observed charge exchange spectrum lines from slowing alpha particles (for example $HeII\ n = 4 - 3$, $\lambda 4685\text{Å}$) are expected to be highly distorted due to Doppler shifts in the line of sight and cross-section effects [17]. The spectrum lines are a measure of the alpha particles at energies $\lesssim 200\text{keV/u}$. This is because of the unavoidable thermal bremsstrahlung background and the falling charge exchange cross-section at high energy. There is an important issue for both diagnostic approaches. The precise beam characteristics and attenuation are essential for quantitative measurements. They are usually evaluated theoretically from the stopping cross-sections and input beam geometry. However the helium beam emission spectrum allows a key *in situ* measurement. For these reasons, beam emission spectroscopy, charge exchange spectroscopy and neutral particle detection are best viewed as mutually supporting diagnostics to be carried out simultaneously in alpha particle measurements.

Charge exchange spectroscopy and beam emission spectroscopy with helium beams are quite new and have some specific problems and opportunities qualitatively different from deuterium beams. This is in plasma impurity ion measurements and field measurements distinct from the specific use in fast alpha particle detection described above. The charge exchange cross-sections to form excited states of hydrogen-like impurity ions allow charge exchange spectroscopy measurement of the impurity ion concentrations. These concentrations must be consistent with the beam attenuation which is a sensitive function of the impurity content. At the same time the excitation cross-sections of the helium beam atoms in collision with the impurity ions give rise to the beam emission spectrum. The beam emission spectrum of helium includes both singlet and triplet lines and characterises the ground and the metastable beam content as well as the attenuation into the plasma. This is an important issue since metastable states $2\ ^1S$ and $2\ ^3S$ are efficient charge exchange donors to quite highly excited states of impurity ions. A significant metastable content can introduce a large correction to impurity concentrations inferred on the assumption of ground state helium donors. The metastable content of helium beams on entry into the plasma has been the subject of some discussion ([18] [19] [20]). For a beam formed by He^+ acceleration, neutralised in He^0, $\lesssim 7\%$ seems likely. The differential attenuation of the ground and metastable populations into the plasma and the regeneration of the metastable populations in the plasma matter. The beam emission

spectrum can clarify this. Since ion collisions cannot cause a spin change in the He^0 by electron exchange, excitation of the triplet side from the singlet side in the plasma must result from electron collisions or from spin system breakdown in higher nl shells. For stationary He^0, the spin system breakdown reaches $\sim 50\%$ for $4f\,^1F$ and $4f\,^3F$ (Van den Eynde [21]) but it must be noted that the motional Stark effect perturbs and mixes l-states significantly. This is particularly so for the $n = 4$ and possible $n = 3$ levels at beam energies $\gtrsim 50\mathrm{keV/u}$.. Collisional radiative redistribution (and ionisation) effects are also pronounced for such levels. Sudden shifts of spectral emission from visible (for example $4\,^1F - 3\,^1D$) to VUV (for example $4\,^1F - 3\,^1D$) wavelengths can occur depending on the mixing. Thus the singlet and triplet side emission is diagnostic of magnetic fields, densities and beam energies within the plasma.

3. ASPECTS OF BERYLLIUM AND BORON AND THEIR MEASUREMENT.

The sources of beryllium and boron are the surfaces with which the plasma interacts. These are the effective limiters, divertor throats and dump plates and the vessel walls. The energy and particle fluxes to the surfaces lead to impurity sputtering and release as neutral atoms or molecules which ionise rapidly as they move into the plasma. Subsequently, they return to the surfaces, generally in highly ionised states. Of special interest at this time is the axisymmetric pumped divertor which seeks to entrap and retain impurities and mimimise their release. High density, low temperature, strongly radiating conditions in the divertor are required, in the creation of which impurity radiation plays an important role. Species such as beryllium and boron are fully ionised over the bulk of the plasma occuring as partially ionised atoms only in the edge plasma. That is in the peripheral confined plasma and in the unconfined scrape-off layer plasma (see Stangeby & McCracken [22] for a comprehensive review of the edge plasma).

The neutral and ion population distributions are usually distinguished since only the latter are tied to the magnetic field. Also the neutral distribution can be markedly non-thermal reflecting it's sputtering or molecular dissociation origin. A further subdivision can be made into the populations of beryllium and boron ions in neutral deuterium rich environments and those where the neutral deuterium concentration is low. The deuterium itself has a number of populations of different velocity distributions and spatial extent, namely molecules, initially dissociated atoms and then the successive charge exchange generations produced in D/D^+ collisions. The low temperature, high density divertor plasma is a region of high neutral deuterium concentration. The relative populations and fluxes of deuterium and impurities are important and observations of impurities and deuterium are usually linked.

In addition to the edge related populations, there are of course the distinct population distributions of Be^{+3} and B^{+4} located in the beam penetrated core plasma core. Be^{+4} and B^{+5} recombine through charge exchange with D^0 or He^0 in the beams. They are reionised in the beam free region where they form part of the plume populations. Apart from these populations, the ionisation state of the beryllium and boron ions depends principally on electron collisions (typical edge temperatures are $\lesssim 200eV$ and the divertor plasma near the target plates may be $\sim 10eV$). Collisional ionisation, radiative and dielectronic recombination are the main processes although the low ionisation stages are generally inflowing in an ionising environment, so recombination is less important. The metastable state populations, such as $Be^0(2s2p\,^3P)$ must be viewed dynamically as well as the ground populations of the ionisation stages. The ionisation and recombination of the neutral and singly

ionised species are affected by stepwise collisional radiative processes. In the deuterium rich regions the ionisation state is modified by charge exchange collisions with neutral deuterium. Ground state deuterium is the principal donor affecting the ionisation balance. The radiated power can be very sensitive to this change. For example, at $5eV \lesssim T_e \lesssim 10eV$ Be^{+2} and B^{+3} are dominant in abundance in an equilibrium plasma, but not radiating. The radiation is by the lithium-like ions Be^{+1} and B^{+2}. Charge exchange enhances the lithium-like stage and the power radiated without changing the dominant ionisation stage [23]. Evidently, generalised collisional-radiative treatment is required to include these points properly in models. This implies extensive need of good fundamental cross-section data.
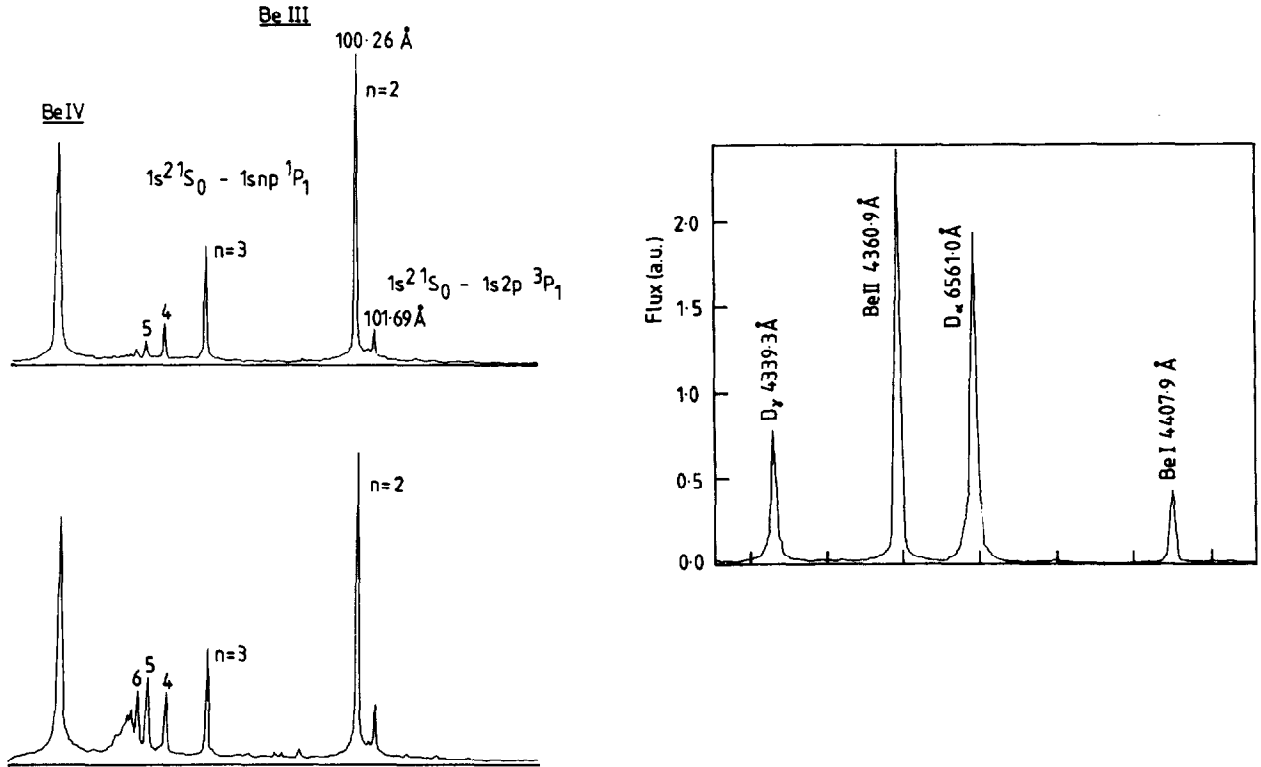

Fig. 2. (a) XUV spectrum along a line of sight directed at the inner wall of JET in the vicinity of the BeIII resonance line when the plasma is in contact with the outer belt limiters. (b) Similar spectrum with the plasma in contact with the inner wall. The difference is attributed to charge exchange with thermal neutral deuterium recycling from the inner wall. The transfer from $D^0(n = 2)$ populates the $Be^{+2}(n \sim 5)$ levels. (c) Spectrum emission from inflowing Be^0 ions at the lower X-point beryllium protected strike zones in JET. The 4407 Å line has a 4 ^1S upper state whose population is strongly affected by redistributing and ionising collisions. Note the conveniently located 2nd. order D_α line in this 3rd. order spectrum.

Turning to measurement, spectroscopy is the primary tool. Objectives are identification of species, observation of geometrical spread of ionisation shells, deduction of fluxes, assessment of metastables and spectrum-line based diagnostics of electron and ion temperatures and electron density. Primary measurements are of the resonance lines. At $\sim 10eV$ the lithium-like lines $BeII\ \lambda 3131$Å and $BIII\ \lambda 2066$Å dominate the radiated power, with the helium like lines at $\sim \lambda 100$Å and $\sim \lambda 60$Å important at $\gtrsim 40eV$. Diagnostic spectroscopy selects additional spectrum lines to identify the contribution of metastable states and to aid deduction of electron temperature and density. There are considerable benefits in visible spectroscopy (principally simple absolute calibration) for studying

emission near localised surfaces and this influences the range of atomic data required. Useful visible radiation generally occurs from transitions amongst the $n = 3$ and $n = 4$ shells. (visible transitions and quartz UV transitions occur to the $n = 2$ shell in the neutrals) for the impurity ions. Also the upper emitting level must not have an allowed transition to the ground state to avoid an unfavourable VUV branch. Thus excitations of dipole, non-dipole and spin change type are all required up to the $n = 4$ shells. The low charge states and relatively high density in divertors mean that redistributive collisions also matter. Evidently the spectral emission requirements and those for the generalised collisional-radiative calculation of ionisation and recombination coefficients are closely connected [24]. Calculated local emissivities in specific lines are often expressed in terms of 'photon efficiencies' or 'ionisations per photon' since these allow immediate interpretation of observed signals as impurity fluxes [25]. It should be noted that collisional-radiative effects make the photon efficiencies electron density as well as temperature sensitive. Electron temperature and density measurements are not readily available in divertor plasma regions and so sensitive line ratios are helpful. In more detailed studies of divertors, calculated local emissivities are incorporated in Monte Carlo models of the impurity ion population distributions for prediction of detailed emission structure. These models are run in close association with neutral deuterium models [26], [22]. There is particular interest at this time in modification of emission by charge transfer in the deuterium rich environment. Excited deuterium (in the $n = 2$ or $n = 3$ shells) is an efficient donor here especially to the higher n-shells of the more highly ionised beryllium and boron ions (see the edge signal observed in charge exchange spectroscopy studies using beams [27] and also [28]). Factors which influence the D^0 ($n = 2$) population are therefore important. In this respect, it is to be noted that optical depth in the Lyman lines in cool high hydrogen density divertor plasma can become large. The implications are still to be appraised.

4. THE REQUIRED CROSS-SECTION DATA FOR HELIUM.

Only fully ionised low and moderate mass ions, in collision with He^0 need to be considered. Of principal importance are the D^+, T^+ fuel and the He^{-2} ash or added minority. Other relevant impurities are due to choices of plasma facing first wall materials and then deposition and gettering strategies. This gives in order of importance C^{+6} (walls, X-point target plates, limiters, carbonisation), Be^{+4} (JET X-point target plates, limiters and evaporation) and B^{+5} (boronisation). The gettering procedures have reduced the importance of oxygen, but nontheless O^{+8} must be included. Other species are of less concern. Titanium, iron and nickel are possible structural materials, neon and argon useful added trace gases for diagnostics, and silicon a possible impurity. A representative set through the second and third period which would act as a basis for interpolation is Ne^{+10}, Si^{+14}, Ar^{+18}, Fe^{+26}.

Concerning energy ranges of cross-section data, since alpha particles are born by deuterium/tritium fusion at 880keV/u, this energy sets the upper limit for He^0 ion/atom stopping cross-sections. The lower limit is set by the beam He^0 particles in collision with thermal plasma ions. A beam energy ~30keV/u (JET ^{4}He beams) and plasma ion temperatures up to 30keV (15keV/u for D^+) would properly set ~1keV/u as the lower limit for ion/atom collision cross-sections. For ITER helium beams , which should certainly have particle energies $\geq$50keV/u, a lower energy limit for cross-sections ~10-20 keV/u is probably acceptable. Electron collisions contribute less to beam stopping. Electron temperatures from 1keV up to 25keV at the plasma core are most relevant. However noting the additional interest of HeI plasma edge and divertor emission for helium recycling

and the helium inventory, the low energy range should be reduced to a few eV. Given the present state of e/He^0 data, it is appropriate now to recommend cross-sections complete in energy from threshold to infinity.

It is appropriate to make a broad statement of minimum accuracy requirements in cross-section data although more specific assessments are made in later contributions. Typically detector calibration, window transmission variation, plasma and viewing geometries, spectral feature isolation and uncertainties in temperature and density profiles limit experimental accuracy to $>40\%$, so this is the acceptable accuracy for modelling prediction of the final observed quantities. Therefore in beam driven diagnostics, 30% error in beam attenuation and 30% error in local particle production coefficients (eg. He^0 by neutralising) or photon effective emission coefficients (eg. by single charge transfer in CXS) calculation is acceptable. Beam attenuation up to a factor 10 is typically encompassed in an experiment, therefore net stopping cross-sections at $<10\%$ accuracy are required. Individual acceptable cross-section tolerances are then in inverse proportion to their contribution. Impurity cross-sections scale at worst as Z^2 and so their acceptable tolerances are in inverse proportion to Z^2 times the fractional impurity abundance. Helium fractional abundance at up to 20% may be expected in fusion plasmas, but experimental test plasmas of pure helium are possible. Carbon and light impurities at $<5\%$ are anticipated. The contribution of each impurity to Zeff is a helpful measure of its importance.

In presenting the following, it has been convenient to allow some repetition of cross-sections so that the different areas can appear complete. A coding (*1) - (*6) has been used to rank importance. Also, a minimum accuracy is suggested as a percentage with an indication of its variation with energy. For beam stopping, the accuracy is based on the proportion of each individual cross-section's contribution and its being the sole source of error. This is of course subject to revision in the light of improvement of our cross-section knowledge and progress in modelling. The least acceptable accuracy is set at 100%. Impurity cross-section accuracies are assessed as though the impurity alone is contributing. Zeff based adjustment of these as described in section 2 is appropriate. For electron collisions, taking account of the many experimental measurements and theoretical calculations 20% accuracy is suggested as a reasonable aspiration at all energies for important transitions.

4.1. Alpha particle neutralisation

This is the essential reaction between beam He^0 and the alpha particle produced by deuterium/tritium fusion which allows the neutral particle diagnostics to probe the alpha particle sources.

He^{+2} neutralisation

(*1) He^0(1^{1}S) + He^{+2} --> He^{+2} + He^0,   20%
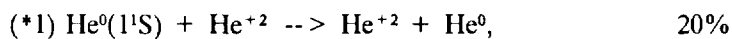
4.2. Beam and fusion He^0 stopping at low density

Most helium is in its ground state so that the dominant stopping is by electron loss directly from the ground state. If the plasma density is very low so that excited helium populations are negligible, this is the only pathway.

9

Ground state single electron loss with primary species and impurities

(*1) $He^0(1^1S)$ + D^+ --> He^+ + D^+ + e,   90% @ 20keV/u, 10% @ > 100keV/u
(*1) $He^0(1^1S)$ + D^+ --> He^+ + D^0,   10% @ 20keV/u, 40% @ > 100keV/u
(*1) $He^0(1^1S)$ + He^{+2} --> He^+ + He^{+2} + e,   100% @ 20keV/u, 20% @ > 100keV/u
(*1) $He^0(1^1S)$ + He^{+2} --> He^{+1} + He^{+1},   20% @ 20keV/u, 20% @ > 100keV/u
(*2) $He^0(1^1S)$ + X^{+z} --> He^+ + X^{+z} + e,   100% @ 20keV/u, 50% @ > 100keV/u
(*2) $He^0(1^1S)$ + X^{+z} --> He^{+1} + X^{+z-1},   10% @ 20keV/u, 20% @ > 100keV/u

With the data at this stage, an approximate stopping can be obtained. However improvement at lower beam energies requires the following:

Ground state double electron loss with primary species and impurities

(*2) $He^0(1^1S)$ + D^+ --> He^{+2} + D^+ + e + e,   100%
(*2) $He^0(1^1)$ + D^+ --> He^{+2} + D^0 + e,   100%
(*2) $He^0(1^1S)$ + He^{+2} --> He^{+2} + He^{+2} + e + e,   100%
(*2) $He^0(1^1S)$ + He^{+2} --> He^{+1} + He^{+1} + e,   100%
(*2) $He^0(1^1S)$ + He^{+2} --> He^{+2} + He^0,   30% @ 20keV/u, 100% @ > 100keV/u
(*3) $He^0(1^1S)$ + X^{+z} --> He^{+2} + X^{+z} + e + e,   80% @ 20keV/u, 40% @ > 100keV/u
(*3) $He^0(1^1S)$ + X^{+z} --> He^{+1} + X^{+z-1} + e,   80% @ 20keV/u, 40% @ > 100keV/u
(*3) $He^0(1^1S)$ + X^{+z} --> He^{+2} + X^{+z-2},   100%

Ground state ionisation by electron impact

(*2) $He^0(1^1S)$ + e --> He^+ + e + e,   20%

4.3. Beam and fusion He^0 stopping at moderate and high density

At plasma densities appropriate to ITER, impact excitation of helium from its ground state to excited states is sufficiently large for the latter populations to be non-negligible. Then electron loss from the excited states can occur before return to the ground. This enhances the stopping. The metastable state (1s2s ^1S and 1s2s ^3S) populations are the most important in this respect, so cross-sections involved in their formation and destruction are the first priority. Thereafter other excited state populations up to an effective cut-off principal quantum shell, at which Lorentz electric field or collisional merging to the continuum occurs, matter.

Ground state excitation to the n= 2 shell by primary species and impurities

(*2) $He^0(1^1S)$ + D^+ --> $He^0(2^1S, 2^1P)$ + D^+,   100%
(*2) $He^0(1^1S)$ + He^{+2} --> $He^0(2^1S, 2^1P)$ + He^{+2},   100%
(*3) $He^0(1^1S)$ + X^{+z} --> $He^0(2^1S, 2^1P)$ + X^{+z},   100%

Ground state excitation to the n= 2 shell by electrons

(*3) $He^0(1^1S)$ + e --> $He^0(2^1S, 2^1P, 2^3S, 2^3P)$ + e,   20%

It is to be noted that ion impact excitations are spin system preserving, while electron collisions allow exchange.

n = 2 state single electron loss with primary species, impurities and electrons

(*2) $He^0(2^{2S+1}L) + D^+ --> He^+ + D^+ + e$,   100%

(*2) $He^0(2^{2S+1}L) + D^+ --> He^+ + D^0$,   100%

(*2) $He^0(2^{2S+1}L) + He^{+2} --> He^+ + He^{+2} + e$,   100%
(includes inner electron ionisation)

(*2) $He^0(2^{2S+1}S) + He^{+2} --> He^{+1} + He^{+1}$,   100%

(*3) $He^0(2^{2S+1}L) + X^{+z} --> He^+ + X^{+z} + e$,   100%
(includes inner electron ionisation)

(*3) $He^0(2^{2S+1}S) + X^{+z} --> He^{+1} + X^{+z-1}$,   100%

(*3) $He^0(2^1S, 2^1P, 2^3S, 2^3P) + e --> He^+ + e + e$,   20%

Redistributive collisions within the n = 2 shell by primary species, impurities and electrons

(*2) $He^0(2^{2S+1}L) + D^+ --> He^0(2^{2S+1}L') + D^+$,   100%

(*2) $He^0(2^{2S+1}L) + He^{+2} --> He^0(2^{2S+1}L') + He^{+2}$,   100%

(*3) $He^0(2^{2S+1}L) + X^{+z} --> He^0(2^{2S+1}L') + X^{+z}$,   100%

(*3) $He^0(2^{2S+1}L) + e --> He^0(2^{2S+1}L') + e$,   20%

With the data at this stage, the 2^1S state populations and enhanced stopping via the singlet side can be obtained approximately. The 2^3S state population is incorrect and requires the following:

Ground state excitation to the $2<n\leq4$ shells by primary species and impurities

(*3) $He^0(1^1S) + D^+ --> He^0(n^1L) + D^+$,   100%

(*3) $He^0(1^1S) + He^{+2} --> He^0(n^1L) + He^{+2}$,   100%

(*4) $He^0(1^1S) + X^{+z} --> He^0(n^1L) + X^{+z}$,   100%

It is to be noted that excitation to 4^1F opens access to the triplet side through state mixing with 4^3F.

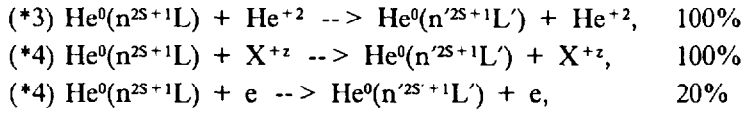*Ground state excitation to the $2<n\leq4$ shell by electrons*

(*3) $He^0(1^1S) + e --> He^0(n^1L, n^3L) + e$,   20%

$2<n\leq4$ state single electron loss with primary species, impurities and electrons

(*3) $He^0(n^{2S+1}L) + D^+ --> He^+ + D^+ + e$,   100%

(*3) $He^0(n^{2S+1}L) + D^+ --> He^+ + D^0$,   100%

(*3) $He^0(n^{2S+1}L) + He^{+2} --> He^+ + He^{+2} + e$,   100%
(includes inner electron ionisation)

(*3) $He^0(n^{2S+1}S) + He^{+2} --> He^{+1} + He^{+1}$,   100%

(*4) $He^0(n^{2S+1}L) + X^{+z} --> He^+ + X^{+z} + e$,   100%
(includes inner electron ionisation)

(*4) $He^0(n^{2S+1}L) + X^{+z} --> He^{+1} + X^{+z-1}$,   100%

(*4) $He^0(n^{2S+1}L) + e --> He^+ + e + e$,   20%

Redistributive collisions between $2\leq n,n'\leq4$ shells by primary species, impurities and electrons

(*3) $He^0(n^{2S+1}L) + D^+ --> He^0(n'^{2S+1}L') + D^+$,   100%

(*3) $He^0(n^{2S+1}L) + He^{+2} \rightarrow He^0(n'^{2S+1}L') + He^{+2}$, 100%

(*4) $He^0(n^{2S+1}L) + X^{+z} \rightarrow He^0(n'^{2S+1}L') + X^{+z}$, 100%

(*4) $He^0(n^{2S+1}L) + e \rightarrow He^0(n'^{2S'+1}L') + e$, 20%

Residual cross-sections up to n= 10 by primary species, impurities and electrons

(*5) $He^0(n) + D^+ \rightarrow He^0(n') + D^+$, 100%

(*5) $He^0(n) + He^{+2} \rightarrow He^0(n') + He^{+2}$, 100%

(*6) $He^0(n) + X^{+z} \rightarrow He^0(n') + X^{+z}$, 100%

(*5) $He^0(n) + e \rightarrow He^0(n') + e$, 20%
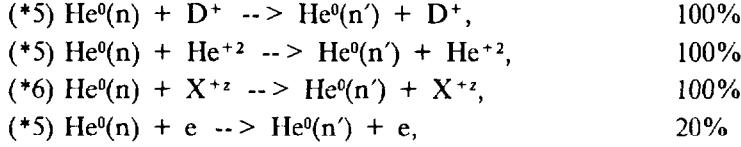
Spin system merging and l-subshell mixing is large beyond n = 4 and merging with the continuum by field ionisation occurs by n = 10 typically.

4.4. Beam emission spectroscopy

Spectral emission from the beams is an important opportunity for experimental verification of beam attenuation and of the correctness of the enhancements attributed to the finite plasma density. Exploitation of the scope of beam emission spectroscopy dictates that emission from helium excited states up to the n = 4 shell should be modelled carefully. For example the transitions 4 ^1L - 2 ^1P are of particular interest since the forbidden components and linear Stark shifts are diagnostic. The overall atomic data requirements are the same as for beam stopping at moderate and high density. However the priority and accuracy for processes populating and depopulating upper states of observable spectrum lines are altered. These are repeated here.

Ground state excitation to the 2<n≤4 shells by primary species and impurities

(*2) $He^0(1^1S) + D^+ \rightarrow He^0(n^1L) + D^+$, 30%

(*2) $He^0(1^1S) + He^{+2} \rightarrow He^0(n^1L) + He^{+2}$, 30%

(*2) $He^0(1^1S) + X^{+z} \rightarrow He^0(n^1L) + X^{+z}$, 30%

Ground state excitation to the 2<n≤4 shell by electrons

(*2) $He^0(1^1S) + e \rightarrow He^0(n^1L, n^3L) + e$, 20%

Initial estimates suggest that 4^1L - 2^1P on the singlet side and 4^3P - 2^3S on the triplet side should be studied experimentally as well as the transitions from the n = 3 shells

2<n≤4 state single electron loss with primary species, impurities and electrons

(*2) $He^0(n^{2S+1}L) + D^+ \rightarrow He^+ + D^+ + e$, 40% @ 20keV/u, 40% @ > 100keV/u
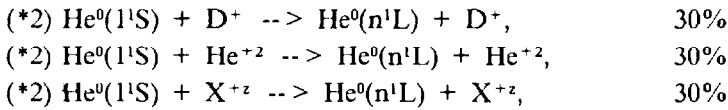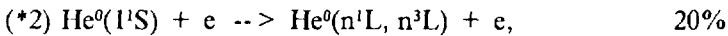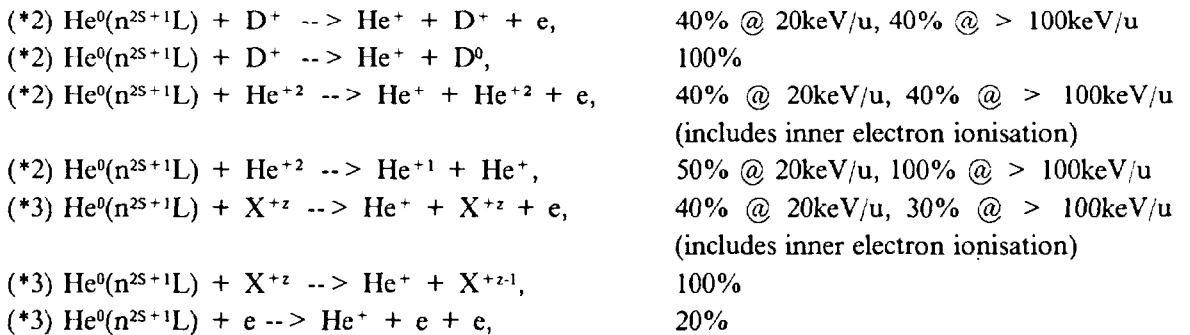
(*2) $He^0(n^{2S+1}L) + D^+ \rightarrow He^+ + D^0$, 100%

(*2) $He^0(n^{2S+1}L) + He^{+2} \rightarrow He^+ + He^{+2} + e$, 40% @ 20keV/u, 40% @ > 100keV/u (includes inner electron ionisation)

(*2) $He^0(n^{2S+1}L) + He^{+2} \rightarrow He^{+1} + He^+$, 50% @ 20keV/u, 100% @ > 100keV/u

(*3) $He^0(n^{2S+1}L) + X^{+z} \rightarrow He^+ + X^{+z} + e$, 40% @ 20keV/u, 30% @ > 100keV/u (includes inner electron ionisation)

(*3) $He^0(n^{2S+1}L) + X^{+z} \rightarrow He^+ + X^{+z-1}$, 100%

(*3) $He^0(n^{2S+1}L) + e \rightarrow He^+ + e + e$, 20%

Redistributive collisions between 2≤n,n'≤4 shells by primary species, impurities and electrons

(*2) $He^0(n^{2S+1}L)$ + D^+ --> $He^0(n'^{2S+1}L')$ + D^+,   30%
(*2) $He^0(n^{2S+1}L)$ + He^{+2} --> $He^0(n'^{2S+1}L')$ + He^{+2},   30%
(*3) $He^0(n^{2S+1}L)$ + X^{+z} --> $He^0(n'^{2S+1}L')$ + X^{+z},   30%
(*3) $He^0(n^{2S+1}L)$ + e --> $He^0(n'^{2S'+1}L')$ + e,   20%
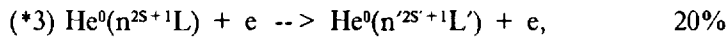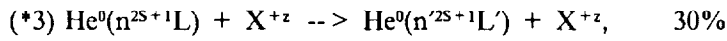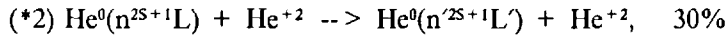
The residual cross-sections of section 4.3 are again required.

4.5. Charge exchange spectroscopy

State selective single electron charge transfer from neutral helium beam atoms in their ground state to alpha particles forming excited states of He^{+1} is the initial concern. Subsequent HeII emission, such as n = 4-3 at 4685A, is the CXS signal to be contrasted with the neutral particle analyser signals. There is a futher aspect however , in that, neutral helium beams may be useable in CXS for all light impurity densities. Consistency with impurity densities used for modelling beam stopping may then be sought.

*State selective charge transfer from ground state to primary species*

(*2) $He^0(1^1S)$ + He^{+2} --> He^+ + $He^+(nl\ ^2L)$,   30%
(*2) $He^0(1^1S)$ + D^+ --> He^+ + $D(nl\ ^2L)$,   30%
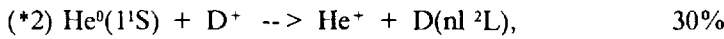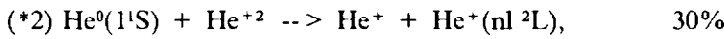
The first is the key reaction for CXS. The second is relevant for formation of the D^0 halo associated with the helium beams. For He, 1≤n≤6, and for D, 1≤n≤4, are relevant ranges.

State selective transfer ionisation from ground state to primary species

(*4) $He^0(1^1S)$ + He^{+2} --> He^{+2} + $He^+(nl\ ^2L)$ + e,   100%
(*4) $He^0(1^1S)$ + D^+ --> He^{+2} + $D(nl\ ^2L)$ + e,   100%
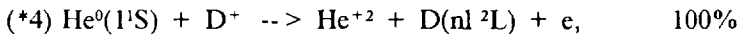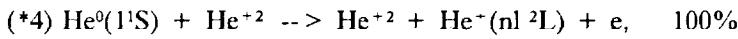
These reactions tend to populate low n shells. They provide a correction of CXS using short wavlength transitions.

State selective charge transfer from metastables to primary species

(*3) $He^0(2^1S, 2^3S)$ + He^{+2} --> He^+ + $He^{+1}(nl\ ^2L)$,   50%
(*3) $He^0(2^1S, 2^3S)$ + D^+ --> He^+ + $D(nl\ ^2L)$,   50%
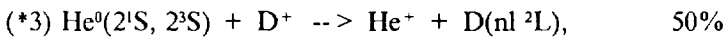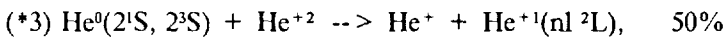
These reactions are most relevant at low beam energies and to CXS with visible lines since the dominant receiving n-shell is usually close to the line emitting n-shell. Expectations of beam metastable populations suggest this may be a significant correction. For He, 1≤n≤6, and for D, 1≤n≤4, are relevant ranges. Redistribution and ionising collisions with the He^+ and D excited populations are required to complete the diagnostic modelling. These are not given explicitly here since He^0 is the main focus.

State selective charge transfer from ground state and metastables to impurities

(*3) $He^0(1^1S)$ + X^{+z0} --> He^+ + $X^{+z0-1}(nl\ ^2L)$,   30%
(*3) $He^0(2^1S, 2^3S)$ + X^{+z0} --> He^+ + $X^{+z0-1}(nl\ ^2L)$.   50%
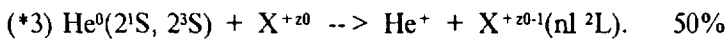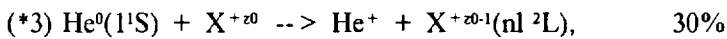
This allows a full CXS diagnostic for impurities using helium beams. The relevant range is $1 \leq n \leq 2z^{0.75}$. Redistribution and ionising collisions with the X^{+z-1} excited populations are required to complete the diagnostic modelling. These are again not given explicitly here.

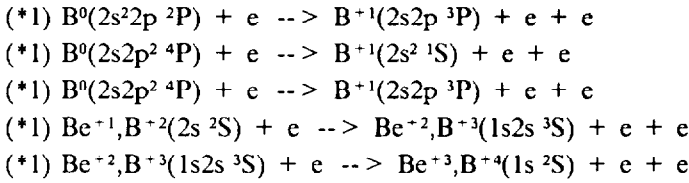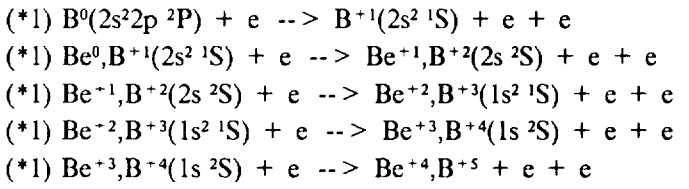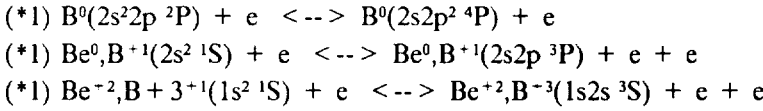## 5. THE REQUIRED CROSS-SECTION DATA FOR BERYLLIUM AND BORON.

5.1. Ionisation state

20% accuracy is appropriate for all the cross-section data in this section. In recombination data, this accuracy applies to the composite zero density coefficient, that is without collisional radiative losses.

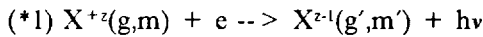*Direct ionisation (ground and metastable) by electron impact*

(*1) $B^0(2s^2 2p\ ^2P) + e \rightarrow B^{+1}(2s^2\ ^1S) + e + e$

(*1) $Be^0, B^{+1}(2s^2\ ^1S) + e \rightarrow Be^{+1}, B^{+2}(2s\ ^2S) + e + e$

(*1) $Be^{+1}, B^{+2}(2s\ ^2S) + e \rightarrow Be^{+2}, B^{+3}(1s^2\ ^1S) + e + e$

(*1) $Be^{+2}, B^{+3}(1s^2\ ^1S) + e \rightarrow Be^{+3}, B^{+4}(1s\ ^2S) + e + e$

(*1) $Be^{+3}, B^{+4}(1s\ ^2S) + e \rightarrow Be^{+4}, B^{+5} + e + e$

(*1) $B^0(2s^2 2p\ ^2P) + e \rightarrow B^{+1}(2s2p\ ^3P) + e + e$

(*1) $B^0(2s2p^2\ ^4P) + e \rightarrow B^{+1}(2s^2\ ^1S) + e + e$

(*1) $B^0(2s2p^2\ ^4P) + e \rightarrow B^{+1}(2s2p\ ^3P) + e + e$

(*1) $Be^{+1}, B^{+2}(2s\ ^2S) + e \rightarrow Be^{+2}, B^{+3}(1s2s\ ^3S) + e + e$

(*1) $Be^{+2}, B^{+3}(1s2s\ ^3S) + e \rightarrow Be^{+3}, B^{+4}(1s\ ^2S) + e + e$

Metastable cross-coefficients by electron impact

(*1) $B^0(2s^2 2p\ ^2P) + e \longleftrightarrow B^0(2s2p^2\ ^4P) + e$

(*1) $Be^0, B^{+1}(2s^2\ ^1S) + e \longleftrightarrow Be^0, B^{+1}(2s2p\ ^3P) + e + e$

(*1) $Be^{+2}, B+3^{+1}(1s^2\ ^1S) + e \longleftrightarrow Be^{+2}, B^{+3}(1s2s\ ^3S) + e + e$

Note that these are not just the direct coefficients but include transfers from the ground or metastable states to excited states of the other spin system and cascade. Accuracies of contributions are pro rata.

Radiative and dielectronic recombination

(*1) $X^{+z}(g,m) + e \rightarrow X^{z-1}(g',m') + h\nu$

g,m and g',m' denote the ground and metastable states of the recombining and recombined systems. The specific reactions are not given explicitly, but the list is the same as in the direct ionisation section above. Note that these are the total zero density coefficients which include the sums over all excited states which cascade to the lowest level of the spin system and include alternative autoionisations. Accuracies of individual components should be pro rata. The sums extend to very high n-shells but there asymptotic behaviour is well specified. The limits to accuracy are in the low level recombination and correct Auger channel opening.

Charge exchange recombination
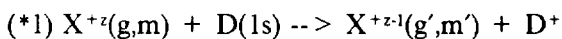
(*1) $X^{+z}(g,m) + D(1s) \rightarrow X^{+z-1}(g',m') + D^+$

Note that these are the total zero density coefficients which include the sums over all excited states which cascade to the lowest level of the spin system but is much more restricted than the dielectronic sums.

Collisional-radiative contributions at finite density

(*2) $X^{+z-1}(g',m')$ + e --> $X^{+z-1}(\{g,m\}n'l'\ ^{2S'+1}L')$ + e (n'≤4)   20%

(*3) $X^{+z-1}(\{g,m\}nl\ ^{2S+1}L)$ + e --> $X^{+z-1}(\{g,m\}n'l'\ ^{2S'+1}L')$ + e   (n,n'≤4)   40%

(*4) $X^{+z-1}(\{g,m\}nl\ ^{2S+1}L)$ + e --> $X^{+z-1}(\{g,m\}n'l'\ ^{2S'+1})$ + e   (n≤4 , n'>4)   40%

(*5) $X^{+z-1}(\{g,m\}nl\ ^{2S+1})$ + e --> $X^{+z-1}(\{g,m\}n'l'\ ^{2S'+1})$ + e (12>n>4 , 12>n'>4)   100%

(*5) $X^{+z-1}(\{g,m\}n\ ^{2S+1})$ + e --> $X^{+z-1}(\{g,m\}n'\ ^{2S'+1})$ + e   (n≥12 , n'≥12)   100%

(*5) $X^{+z-1}(\{g,m\}nl\ ^{2S+1})$ + Z_0 --> $X^{+z-1}(\{g,m\}n'l'\ ^{2S'+1})$ + Z_0 (12>n>4 , 12>n'>4)   100%

(*5) $X^{+z-1}(\{g,m\}n\ ^{2S+1})$ + Z_0 --> $X^{+z-1}(\{g,m\}n'\ ^{2S'+1})$ + Z_0 (n≥12 , n'≥12)   100%

Z_0 denotes fully ionised species . This data is required for the finite density improvement in generalised collisional radiative modelling. It applies also to sections below and is only repeated if higher accuracy is required. Note the changing angular resolution level on moving to higher n-shells. Such nl- and n- bundling while retaining spin systems is an approach of sufficient accuracy. For generalised collisional-radiative recombination and ionisation coefficients, the bundle-n approach can be used for corrections to the direct rates down to the n=2 shell and, for corrections to low level emissivities, down to the n=4 shell. The extension to n ~12 is necessary for high n-shell visible charge exchange spectroscopy where l-mixing matters. The various possible parent states, denoted by g,m must be treated as well as the different spin systems.

5.2. Measurement of total power and low resonance lines

(*1) $X^{+z-1}(g',m')$ + e --> $X^{+z-1}(\{g,m\}n'l'\ ^{2S'+1}L')$ + e (n'≤4)   20%

These cross-sections give the dominant spectral line power at zero density. Recombination contributions, which are much smaller except for the helium-like and hydrogen-like ions at high temperatures, follow from the data in section 5.1. Note that no distinction need be made into the actual cascade paths in the case of power.

5.3. Visible influx spectroscopy

(*1) $X^{+z-1}(g',m')$ + e --> $X^{+z-1}(\{g,m\}n'l'\ ^{2S'+1}L')$ + e (n'≤4)   20%

(*2) $X^{+z-1}(\{g,m\}nl\ ^{2S+1}L)$ + e --> $X^{+z-1}(\{g,m\}n'l'\ ^{2S'+1}L')$ + e   (n,n'≤4)   30%

This is a repeat of the collisional-radiative part of section 5.1 but higher accuracy is necessary. This data allows the low level excitation and redistribution part of line emissivities to be obtained. Recombination contributions to emissivities and stepwise collisional radiative losses through higher levels requires the additional data of section 5.1. These are appropriate for highly transient and dense plasma conditions.

5.4. Charge exchange spectroscopy

State selective CX into excited shells for influx ions

(*1) X^{+z}(g,m) + D(1s) --> X^{z-1}({g,m}nl ^{2S+1}L) + D^{+} 30%

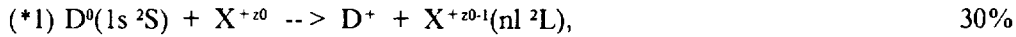(*1) X^{+z}(g,m) + D(n = 2,3) --> X^{z-1}({g,m}nl ^{2S+1}L) + D^{+} 50%
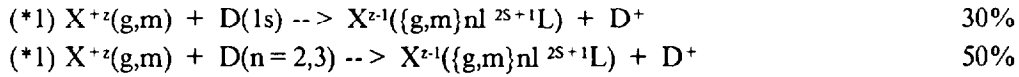
The redistributive collisional data required in sections 5.2, 5.3 and 5.4 are the same.

Neutral helium beam induced

[This is given in section 4.5.]

Neutral deuterium beam induced

(*1) D^{0}(1s ^{2}S) + X^{+z0} --> D^{+} + X^{+z0-1}(nl ^{2}L), 30%

This allows a full CXS diagnostic for impurities using deuterium beams. The relevant range is $1 \leq n \leq 2z^{0.75}$. Redistributive collisional data are also required (see section 4.5).

6. CONCLUSIONS

We have sought to lay out the set of atomic collision cross-section data required to model and support alpha particle diagnostics for ITER and other fusion experiments using neutral helium beams. However, we have gone further in that we have also addressed the data required in practise to support and validate such a diagnostic fully by associating it with charge exchange and beam emission spectroscopy. Secondly, we have laid down the atomic data needs for beryllium and boron in divertor experiments. It is anticipated that the data will form the high quality input to comprehensive excited population, effective ionisation coefficient and effective emissivity coefficient codes in the collisional-radiative sense. There remain some anxieties. As has been mentioned, fast neutral helium atoms in tokamak plasmas will experience a strong vxB electric field establishing a Stark state structure. Whether this can alter the balance of atomic reactions significantly is largely unexplored. Also assumptions of isotropic averages of collision cross-sections cannot really be sustained. We therefore anticipate some elaboration or at least clarification of these points.

REFERENCES

[1] THOMAS, P. R. Nucl. Mater. 176-177 (1990) 3.

[2] WINTER, J., ESSER, H.G., KONEN, L. et al. J. Nucl. Mater. 162-164 (1989) 713 .

[3] HOGAN, J.T. & HILLIS, D.L. Nuclear Fusion 31 (1991) 2181.

[4] REDI, M.H., COHEN, S.A. & SYNAKOWSKI, E.J. Nuclear Fusion 31 (1991) 1689.

[5] JANEV, R.K., LANGER, W.D., EVANS, K. & POST, D.E. (1987) 'Elementary Processes in Hydrogen-Helium Plasmas' (Publ.- Springer-Verlag, Belin).

[6] JANEV, R.K., HARRISON, M.F.A. & DRAWIN, H.W. Nuclear Fusion 29 (1989) 109.

[7] SCHWEER, B., MANK, G., POSPIESZCZYK, A. et al. Europhys. Conf. Abstracts 15 (1991) 361.

[8] MARCUS, F.B., ADAMS, J.M., BARTLETT, D.V. et al. Plasma Phys. Contr. Fusion (1992) - in press. (Also JET-P(92)11).

[9] TOBITA, K., KUSAMA, Y., NAKAMURA, H. et al.. Nuclear Fusion 31 (1991) 956.

[10] KAMELANDER, G. & SIGMAR, D.J. Physica Scripta 45 (1992) 147.

[11] ERIKSSON, L.G., HELLSTON, T., BOYD, D.A. et al. Nuclear Fusion 29 (1989) 87 .

[12] SUMMERS, H.P., VON HELLERMANN, M., BREGER, P., FRIELING, J., HORTON, L.D., KONIG, R., MANDL, W., MORSI, H., WOLF, R., DE HEER, F., HOEKSTRA, R. & FRITSCH, W. Jet Joint Undertaking Report JET-P(91)48 (1991).

[13] FONCK, R.J., DARROW, D.S. & JAEHNIG, R.P. Phys. Rev. **A29** (1984) 3288.

[14] JOBES, F.C., REDI, M.H., ROQUEMORE, A.L. et al. Rev. Sci. Instrum. **61** (1990) 2981.

[15] FISHER, R.K. Rev. Sci. Instrum. (1992) - in press.

[16] PETROV, M.P., AFANASYEV, V.I., CORTI, S. A., GONDALEKAR, A. (1992) Int. Conf. Plasma Physics, Innsbruck, Austria - preprint

KHUDOLEEV, A.V., AFANASYEV, V.I., CORTI, S. A., GONDALEKAR, A., MAAS, A.C. & PETROV, M.P. (1992) Int. Conf. Plasma Physics, Innsbruck, Austria - preprint

[17] VON HELLERMANN, M., MANDL, W., SUMMERS, H.P., BOILEAU, A., HOEKSTRA, R. DE HEER, F., HOEKSTRA, R. & FRIELING, J. Plasma Phys. Contr. Fusion **33** (1991) 1805.

[18] GILBODY, H.B., DUNN, K.F., BROWNING, R & LATIMER, C.J. J. Phys. B. **4** (1971) 800 .

MCCULLOUGH, R.W., GOFFE, T.V. & GILBODY, H.B., J. Phys. B. **11** (1978) 2333 .

[19] TOBITA, K., ITOH, T., SAKASAI, A., KUSAMA, Y., OHARA, Y., TSUKAHARA, Y., NEMOTO, M., KAWANO, Y., KUBO, H., TAKEUCHI, H. & SUGIE, T Plasma Phys. Contr. Fusion **32** (1990) 429.

[20] HEMSWORTH, R. & TRAYNOR, N. JET Joint Undertaking Internal Report (1990) JET-DN-C(90)86.

HOEKSTRA, R., DE HEER, F.J. & MORGENSTERN, R. - unpublished

[21] VAN DEN EYNDE, R.K., WEIBES, G. & NIEMEYER, TH. Physica **59** (1972) 401 .

[22] STANGEBY, P.C. & McCRACKEN, G.M. Nuclear Fusion **30** (1990) 225.

[23] VON HELLERMANN, M. & SUMMERS, H.P. Rev. Sci. Instrum. (1992) - in press.

[24] SUMMERS, H. P., DICKSON, W.J., BOILEAU, A., BURKE, P.G., DENNE-HINNOV, B., FRITSCH, W., GIANNELLA, R., HAWKES, N.C., VON HELLERMANN, M., MANDL, W., PEACOCK, N.J., REID, R.H.G., STAMP, M.F. & THOMAS, P.R. Plasma Phys. Contr. Fusion **34** (1991) 325 .

[25] BEHRINGER, K., SUMMERS, H. P., DENNE, B., FORREST, M. & STAMP, M.F. Plasma Phys. Contr. Fusion **31** (1989) 2059.

[26] KEILHACKER, M., SIMONINI, R., TARONI, A. & WATKINS, M.L. Nuclear Fusion **31** (1991) 535.

[27] BOILEAU, A., VON HELLERMANN, M., HORTON, L.D., SPENCE, J. & SUMMERS, H.P. Plasma Phys. Contr. Fusion **31** (1989) 779.

[28] MATTIOLI, M., PEACOCK, N.J., SUMMERS, H.P., DENNE, B. & HAWKES, N.C. Phys. Rev. **A40** (1989) 3886.

ANNEX

P.-H. REBUT, A. GIBSON, M. HUGUET, J.M. ADAMS[1], B. ALPER, H. ALTMANN, A. ANDERSEN[2], P. ANDREW[3],
M. ANGELONE[4], S. ALI-ARSHAD, P. BAIGGER, W. BAILEY, B. BALET, P. BARABASCHI, P. BARKER, R. BARNSLEY[5],
M. BARONIAN, D.V. BARTLETT, L. BAYLOR[6], A.C. BELL, G. BENALI, P. BERTOLDI, E. BERTOLINI, V. BHATNAGAR,
A.J. BICKLEY, D. BINDER, H. BINDSLEV[2], T. BONICELLI, S.J. BOOTH, G. BOSIA, M. BOTMAN, D. BOUCHER,
P. BOUCQUEY, P. BREGER, H. BRELEN, H. BRINKSCHULTE, D. BROOKS, A. BROWN, T. BROWN, M. BRUSATI,
S. BRYAN, J. BRZOZOWSKI[7], R. BUCHSE[22], T. BUDD, M. BURES, T. BUSINARO, P. BUTCHER, H. BUTTGEREIT,
C. CALDWELL-NICHOLS, D.J. CAMPBELL, P. CARD, G. CELENTANO, C.D. CHALLIS, A.V. CHANKIN[8], A. CHERUBINI,
D. CHIRON, J. CHRISTIANSEN, P. CHUILON, R. CLAESEN, S. CLEMENT, E. CLIPSHAM, J.P. COAD, I.H. COFFEY[9],
A. COLTON, M. COMISKEY[10], S. CONROY, M. COOKE, D. COOPER, S. COOPER, J.G. CORDEY, W. CORE, G. CORRIGAN,
S. CORTI, A.E. COSTLEY, G. COTTRELL, M. COX[11], P. CRIPWELL[12], O. Da COSTA, J. DAVIES, N. DAVIES, H. de BLANK,
H. de ESCH, L. de KOCK, E. DEKSNIS, F. DELVART, G.B. DENNE-HINNOV, G. DESCHAMPS, W.J. DICKSON[13], K.J. DIETZ,
S.L. DMITRENKO, M. DMITRIEVA[14], J. DOBBING, A. DOGLIO, N. DOLGETTA, S.E. DORLING. P.G. DOYLE, D.F. DÜCHS,
H. DUQUENOY, A. EDWARDS, J. EHRENBERG, A. EKEDAHL, T. ELEVANT[7], S.K. ERENTS[11], L.G. ERIKSSON,
H. FAJEMIROKUN[12], H. FALTER, J. FREILING[15], F. FREVILLE, C. FROGER, P. FROISSARD, K. FULLARD, M. GADEBERG,
A. GALETSAS, T. GALLAGHER, D. GAMBIER, M. GARRIBBA, P. GAZE, R. GIANNELLA, R.D. GILL, A GIRARD,
A. GONDHALEKAR, D. GOODALL[11], C. GORMEZANO, N.A. GOTTARDI, C. GOWERS, B.J. GREEN, B. GRIEVSON, R. HAANGE,
A. HAIGH, C.J. HANCOCK, P.J. HARBOUR, T. HARTRAMPF, N.C. HAWKES[11], P. HAYNES[11], J.L. HEMMERICH, T. HENDER[11],
J. HOEKZEMA, D. HOLLAND, M. HONE, L. HORTON, J. HOW, M. HUART, I. HUGHES, T.P. HUGHES[10], M. HUGON, Y. HUO[16],
K. IDA[17], B. INGRAM, M. IRVING, J. JACQUINOT, H. JAECKEL, J.F. JAEGER, G. JANESCHITZ, Z. JANKOVICZ[18], O.N. JARVIS,
F. JENSEN, E.M. JONES, H.D. JONES, L.P.D.F. JONES, S. JONES[19], T.T.C. JONES, J.-F. JUNGER, F. JUNIQUE, A. KAYE,
B.E. KEEN, M. KEILHACKER, G.J. KELLY, W. KERNER, A. KHUDOLEEV[21], R. KONIG, A. KONSTANTELLOS, M. KOVANEN[20],
G. KRAMER[15], P. KUPSCHUS, R. LÄSSER, J.R. LAST, B. LAUNDY, L. LAURO-TARONI, M. LAVEYRY, K. LAWSON[11],
M. LENNHOLM, J. LINGERTAT[22], R.N. LITUNOVSKI, A. LOARTE, R. LOBEL, P. LOMAS, M. LOUGHLIN, C. LOWRY, J. LUPO,
A.C. MAAS[15], J. MACHUZAK[19], B. MACKLIN, G. MADDISON[11], C.F. MAGGI[23], G. MAGYAR, W. MANDL[22], V. MARCHESE,
G. MARCON, F. MARCUS, J. MART, D. MARTIN, E. MARTIN, R. MARTIN-SOLIS[24], P. MASSMANN, G. MATTHEWS,
H. McBRYAN, G. McCRACKEN[11], J. McKIVITT, P. MERIGUET, P. MIELE, A. MILLER, J. MILLS, S.F. MILLS, P. MILLWARD,
P. MILVERTON, E. MINARDI[4], R. MOHANTI[25], P.L. MONDINO, D. MONTGOMERY[26], A. MONTVAI[27], P. MORGAN,
H. MORSI, D. MUIR, G. MURPHY, R. MYRNÄS[28], F. NAVE[29], G. NEWBERT, M. NEWMAN, P. NIELSEN, P. NOLL,
W. OBERT, D. O'BRIEN, J. ORCHARD, J. O'ROURKE, R. OSTROM, M. OTTAVIANI, M. PAIN, F. PAOLETTI,
S. PAPASTERGIOU, W. PARSONS, D. PASINI, D. PATEL, A. PEACOCK, N. PEACOCK[11], R.J.M. PEARCE, D. PEARSON[12],
J.F. PENG[16], R. PEPE DE SILVA, G. PERINIC, C. PERRY, M. PETROV[21], M.A. PICK, J. PLANCOULAINE, J.-P POFFÉ,
R. PÖHLCHEN, F. PORCELLI, L. PORTE[13], R. PRENTICE, S. PUPPIN, S. PUTVINSKII[8], G. RADFORD[30], T. RAIMONDI,
M.C. RAMOS DE ANDRADE, R. REICHLE, J. REID, S. RICHARDS, E. RIGHI, F. RIMINI, D. ROBINSON[11], A. ROLFE,
R.T. ROSS, L. ROSSI, R. RUSS, P. RUTTER, H.C. SACK, G. SADLER, G. SAIBENE, J.L. SALANAVE, G. SANAZZARO,
A. SANTAGIUSTINA, R. SARTORI, C. SBORCHIA, P. SCHILD, M. SCHMID, G. SCHMIDT[31], B. SCHUNKE, S.M. SCOTT,
L. SERIO, A SIBLEY, R. SIMONINI, A.C.C. SIPS, P. SMEULDERS, R. SMITH, R. STAGG, M. STAMP, P. STANGEBY[3],
R. STANKIEWICZ[32], D.F. START, C.A. STEED, D. STORK, P.E. STOTT, P. STUBBERFIELD, D. SUMMERS, H. SUMMERS[13],
L. SVENSSON, J.A. TAGLE[33], M. TALBOT, A. TANGA, A. TARONI, C. TERELLA, A TERRINGTON, A TESINI, P.R. THOMAS,
E. THOMPSON, K. THOMSEN, F. TIBONE, A. TISCORNIA, P. TREVALION, B. TUBBING, P. VAN BELLE, H. VAN DER BEKEN,
G. VLASES, M. VON HELLERMANN, T. WADE, C. WALKER, R. WALTON[31], D. WARD, M.L. WATKINS, N. WATKINS,
M.J. WATSON, S. WEBER[34], J. WESSON, T.J. WIJNANDS, J. WILKS, D. WILSON, T. WINKEL, R. WOLF, D. WONG,
C. WOODWARD, Y. WU[35], M. WYKES, D. YOUNG, I.D. YOUNG, L. ZANNELLI, A. ZOLFAGHARI[19], W. ZWINGMANN

[1] Harwell Laboratory, UKAEA, Harwell, Didcot, Oxfordshire, UK.
[2] Risø National Laboratory, Roskilde, Denmark.
[3] Institute for Aerospace Studies, University of Toronto, Downsview, Ontario, Canada.
[4] ENEA Frascati Energy Research Centre, Frascati, Rome, Italy.
[5] University of Leicester, Leicester, UK.
[6] Oak Ridge National Laboratory, Oak Ridge, TN, USA.
[7] Royal Institute of Technology, Stockholm, Sweden.
[8] I.V. Kurchatov Institute of Atomic Energy, Moscow, Russian Federation.
[9] Queens University, Belfast, UK.
[10] University of Essex, Colchester, UK.
[11] Culham Laboratory, UKAEA, Abingdon, Oxfordshire, UK.
[12] Imperial College of Science, Technology and Medicine, University of London, London, UK.
[13] University of Strathclyde, Glasgow, UK.
[14] Keldysh Institute of Applied Mathematics, Moscow, Russian Federation.
[15] FOM-Institute for Plasma Physics "Rijnhuizen", Nieuwegein, Netherlands.
[16] Institute of Plasma Physics, Academia Sinica, Hefei, Anhui Province, China.
[17] National Institute for Fusion Science, Nagoya, Japan.
[18] Soltan Institute for Nuclear Studies, Otwock/Świerk, Poland.
[19] Plasma Fusion Center, Massachusetts Institute of Technology, Boston, MA, USA.
[20] Nuclear Engineering Laboratory, Lappeenranta University, Finland.
[21] A.F. Ioffe Physico-Technical Institute, St. Petersburg, Russian Federation.
[22] Max-Planck-Institut für Plasmaphysik, Garching, Germany.
[23] Department of Physics, University of Milan, Milan, Italy.
[24] Universidad Complutense de Madrid, Madrid, Spain.
[25] North Carolina State University, Raleigh, NC, USA.
[26] Dartmouth College, Hanover, NH, USA.
[27] Central Research Institute for Physics, Budapest, Hungary.
[28] University of Lund, Lund, Sweden.
[29] Laboratorio Nacional de Engenharia e Tecnologia Industrial, Sacavem, Portugal.
[30] Institute of Mathematics, University of Oxford, Oxford, UK.
[31] Princeton Plasma Physics Laboratory, Princeton University, Princeton, NJ, USA.
[32] RCC Cyfronet, Otwock/Świerk, Poland,
[33] Centro de Investigaciones Energéticas, Medioambientales y Tecnológicas, Madrid, Spain.
[34] Freie Universität, Berlin, Germany.
[35] Insitute for Mechanics, Academia Sinica, Beijing, China.